Generating two-spin squeezed states of separated Bose-Einstein condensates

Juan E. Aristizabal-Zuluaga *,[1,2,3] Iuliia Skobleva,[2] Lars Richter †,[2] Yangxu Ji,[1,2] Yuping Mao,[1,2] Manikandan Kondappan,[1,2] Valentin Ivannikov,[2,4] and Tim Byrnes[2,1,4,5,6,‡]

[1] *State Key Laboratory of Precision Spectroscopy, School of Physical and Material Sciences, East China Normal University, Shanghai 200062, China*
[2] *New York University Shanghai, 1555 Century Ave, Pudong, Shanghai 200122, China*
[3] *Grupo de Física Atómica y Molecular, Instituto de Física, Facultad de Ciencias Exactas y Naturales, Universidad de Antioquia UdeA, Calle 70 No. 52-21, Medellín, Colombia*
[4] *NYU-ECNU Institute of Physics at NYU Shanghai, 3663 Zhongshan Road North, Shanghai 200062, China*
[5] *National Institute of Informatics, 2-1-2 Hitotsubashi, Chiyoda-ku, Tokyo 101-8430, Japan*
[6] *Department of Physics, New York University, New York, NY 10003, USA*

(Dated: June 30, 2020)

We theoretically study a scheme for generating squeezing between two Bose-Einstein condensates (BECs). The scheme involves placing two BECs in the path of a Mach-Zehnder interferometer, where the coherent light interacts with the atoms due to the ac Stark shift. The most relevant regime for producing squeezing is in the short time regime, defined as when the interaction time scales as the inverse square root of the atom number. In this regime it is possible to construct a very simple approximate theory for the overall effect of the scheme: amplitudes in the superposition between the two BECs with unequal spin eigenvalues are damped. We analyze the types of correlations, entanglement, Einstein-Podolsky-Rosen (EPR) steering, and Bell correlations that are produced and show that the state is similar to a spin-EPR state. Using a two-pulse sequence the correlations can be dramatically improved, where the state further approaches a spin-EPR state.

I. INTRODUCTION

Squeezed states [1–4] have played a central role in the development of quantum optics and its applications such as quantum metrology [5–7]. A squeezed state has the property that the quantum fluctuations of an quadrature observable is reduced below that of a coherent state. According to the Heisenberg uncertainty principle, such squeezing is then accompanied by another conjugate observable which is anti-squeezed. Squeezed states of light have been widely studied experimentally and realized using a variety of techniques [8–12], and numerous applications have been proposed [13–18]. Analogously to optical squeezed states, the reduction of quantum noise has also been investigated in other systems, notably in atomic systems. For atomic systems, the relevant degrees of freedom are the internal spin levels, and squeezing occurs if the spin noise fluctuations are below that of a spin coherent state [19–25]. Different types of interactions produce different types of squeezed states, the most well-known being the one-axis and two-axis countertwisting Hamiltonians [26]. Various theoretical schemes for generating squeezing in atomic ensembles have been proposed [27–31], and experimental squeezing has been demonstrated on atomic ensembles and Bose-Einstein condensates [32–48].

Squeezed states involving two or more physical systems have a particular importance in a quantum information contexts. Two-mode squeezed states produce EPR (Einstein-Podolsky-Rosen) correlated states, which show correlations in position variables and anti-correlations in momentum variables. Such states are central in quantum information applications [49, 50], in particular continuous variable quantum computing [51], since they are an entangled states which can be viewed as a resource. In an atomic context, the first demonstrations by Polzik and co-workers showed that two-mode squeezed states could be produced [41, 52, 53], which was followed by various other techniques. For BECs, currently there have not been any demonstrations showing entanglement between two completely separated atomic clouds, but entanglement has been detected between different spatial regions of the same BEC [54–56]. Numerous theoretical proposals have been investigated for generating entanglement between BECs [57–63]. The two-spin generalization of the one-axis and two-axis squeezed states have been theoretically investigated, which shows the nature of the quantum state that is generated by the one-axis two-spin (1A2S) [64, 65] and two-axis two-spin (2A2S) Hamiltonians [66]. Such entangled spin states are anticipated to play a central role in quantum information applications [67, 68].

In this paper, we study an experimental scheme that can be used to generate entanglement between two BECs. In the scheme, coherent light is arranged in a Mach-Zehnder interferometer and two BECs are placed in the two arms of the interferometer (Fig. 1). The light interacts via an ac Stark shift interaction, and after a measurement of the optical state, the two BECs are projected into an entangled state. The scheme has similarities with the

*orcid.org/0000-0001-9775-6282
†orcid.org/0000-0003-0819-9248
‡Electronic address: tim.byrnes@nyu.edu

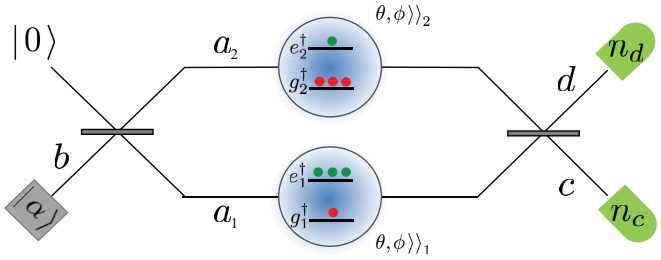

FIG. 1: Experimental scheme for two-spin squeezed generation between two BECs. Coherent light is generated in mode b and enters a beam splitter to emerge as two modes a_j, $j \in \{1,2\}$. Each mode interacts with a BEC due to the ac Stark shift. Each BEC has two internal states, labeled as g_j, e_j. The modes are then interfered again to produce two new modes c, d, and detected using photodetectors measuring in the Fock basis with outcomes n_c and n_d respectively.

scheme introduced in Refs. [52, 62, 69] but has a different geometry, since light passes sequentially through the two atomic clouds in these works. The Mach-Zehnder configuration is more convenient for entangling well-separated BECs. Furthermore, in the context of atomic ensembles [52, 69], the theory generally works within a Holstein-Primakoff approximation, such that the spins are considered to be approximate quadrature operators. Here we use exact techniques which allow us to handle any number of atoms and any interaction time. In contrast to the approaches of Refs. [52, 62, 69], where it was showed that a two-mode squeezed state is generated, using our methods we clarify several key differences. For example, the variance of particular pairs of variables saturate at a finite value, or even increase due to the interactions. The detailed understanding of the protocol allows for us to easily propose a scheme to overcome this, improving the level of squeezing considerably.

This paper is structured as follows. We first derive a theory to describe the entanglement protocol, where we obtain the final wavefunction after the scheme (Sec. II). We find that in the short-time regime there is a convenient approximate method to describe the effect of the light-matter interaction, which gives an effective wavefunction that accurately captures the nature of the state (Sec. III). After briefly describing some elementary properties of the approximate state (Sec. III C), we go on to numerically study the exact state, examining key properties such as the variances, expectation values, entanglement, probability distributions, correlation based entanglement and EPR steering detection, and Bell correlations (Sec. IV). Finally, we show that there is a way to further improve the squeezing properties of the state by repeating the protocol twice (Sec. V). We finally summarize our finding and conclude (Sec. VI).

II. EXPERIMENTAL SCHEME

A. Physical system and Hamiltonian

We first describe the physical system that we consider in this paper. Figure 1 shows the overall scheme. We consider two BECs that are each in well-separated traps. These could be for example two BECs in separate magnetic traps on an atom chip, or two BECs in optical dipole traps [70–72]. Each of the BECs have two internal energy states that can be populated, for which the bosonic annihilation operators are g_j, e_j, where $j \in \{1,2\}$ labels the two BECs. The two internal states could be for example the $F = 1, m_F = -1$ and $F = 2, m_F = 1$ clock states in the case of ^{87}Rb [42, 44, 54, 73]. It is convenient to construct Schwinger boson operators

$$\begin{aligned} S_j^x &= e_j^\dagger g_j + g_j^\dagger e_j, \\ S_j^y &= -ie_j^\dagger g_j + ig_j^\dagger e_j, \\ S_j^z &= e_j^\dagger e_j - g_j^\dagger g_j. \end{aligned} \tag{1}$$

which have commutation relations $[S^i, S^j] = 2i\epsilon_{ijk}S^k$ where ϵ_{ijk} is the completely antisymmetric Levi-Civita tensor. We consider here that the total number of atoms is fixed for each BEC, such that

$$g_j^\dagger g_j + e_j^\dagger e_j = N. \tag{2}$$

The states of a BEC can be written in terms of Fock states, defined as

$$|k\rangle = \frac{(e^\dagger)^k (g^\dagger)^{N-k}}{\sqrt{k!(N-k)!}}|\text{vac}\rangle, \tag{3}$$

where $|\text{vac}\rangle$ is the state with no atoms or photons. We also use the notation for spin coherent states

$$|\theta,\phi\rangle\rangle \equiv \frac{1}{\sqrt{N!}}\left(e^\dagger \cos\frac{\theta}{2} + g^\dagger \sin\frac{\theta}{2}e^{i\phi}\right)^N |\text{vac}\rangle, \tag{4}$$

where $0 \le \theta \le \pi$, $-\pi \le \phi \le \pi$ are spherical angles on the Bloch sphere.

Two optical modes interact with the each of the BECs, in a Mach-Zehnder configuration as shown in Fig. 1. The bosonic annihiliation operator for the mode that the laser initially illuminates is called b. This mode enters a beam splitter, which transforms the mode according to

$$b = \frac{1}{\sqrt{2}}(a_1 + a_2) \tag{5}$$

where the bosonic annihilation operators for each mode passing through BEC 1 and 2 are a_1, a_2 respectively. Defining Stokes operators for the optical modes in the dual-rail encoding, we have

$$\begin{aligned} J^z &= a_1^\dagger a_1 - a_2^\dagger a_2 \\ n &= a_1^\dagger a_1 + a_2^\dagger a_2 \end{aligned} \tag{6}$$

where n is the number operator for photons. After passing through the two BECs, the photons are incident upon a beam splitter which transforms the modes according to

$$a_1 = \frac{1}{\sqrt{2}}(c+d)$$
$$a_2 = \frac{1}{\sqrt{2}}(c-d). \tag{7}$$

The states of the light are written in terms of Fock states

$$|n\rangle_b = \frac{(b^\dagger)^n}{\sqrt{n!}}|\text{vac}\rangle. \tag{8}$$

Coherent states are implied from the use of a single Greek symbol

$$|\alpha\rangle_b \equiv e^{-|\alpha|^2/2} e^{\alpha b^\dagger}|\text{vac}\rangle. \tag{9}$$

The atoms within the BECs interact with the light due to an ac Stark shift interaction [74–78]

$$H = \frac{\hbar\Omega}{2}\left(S_1^z - S_2^z\right) J^z. \tag{10}$$

The spin-dependence of the interaction occurs because the selection rules of the transition with respect to the hyperfine ground states only produce an ac Stark shift for one of the states g_j, e_j [77]. We will work in the rotating frame of the spins such that any rotation caused by diagonal terms in the Hamiltonian are accounted for. After the interaction with the light, the two modes are interfered and the number of photons in the modes c, d are measured. We will show in the following section that this results in an entangled state between the BECs.

B. Dynamics

We now derive the state that is produced by the sequence shown in Fig. 1. In our derivation we consider a general initial state of the BECs, given by

$$|\Psi_0\rangle = \sum_{k_1,k_2=0}^{N} \Psi_{k_1k_2}|k_1\rangle|k_2\rangle. \tag{11}$$

A suitable choice of initial state are two BECs that are polarized in the S^x-direction,

$$|\Psi_0\rangle = \left|\frac{\pi}{2}, 0\right\rangle\!\!\right\rangle_1 \left|\frac{\pi}{2}, 0\right\rangle\!\!\right\rangle_2 \tag{12}$$

which can be expanded in the Fock basis such that

$$\Psi_{k_1k_2} = \frac{1}{2^N}\sqrt{\binom{N}{k_1}\binom{N}{k_2}}. \tag{13}$$

Throughout this paper, we will generally consider the initial state (12) unless otherwise stated.

The laser illuminates the mode b in a coherent state, such that the initial state of photons is given by $|\alpha\rangle_b$. After the first beam splitter, the initial state is thus

$$|\psi(0)\rangle = |\Psi_0\rangle \left|\frac{\alpha}{\sqrt{2}}\right\rangle\!\!\right\rangle_{a_1} \left|\frac{\alpha}{\sqrt{2}}\right\rangle\!\!\right\rangle_{a_2}. \tag{14}$$

The light now interacts with the BECs. We assume that the light interacts for a time t with the BECs, such that the state after it passes the BECs becomes

$$|\psi(\tau)\rangle = e^{-iHt/\hbar}|\psi(0)\rangle \tag{15}$$
$$= \exp\left[-\frac{i\tau}{2}\left(S_1^z - S_2^z\right)J^z\right]|\psi(0)\rangle$$

where we have defined the dimensionless time $\tau \equiv \Omega t$. Substituting (14) with (11) gives

$$|\psi(\tau)\rangle = \sum_{k_1,k_2=0}^{N} \Psi_{k_1k_2}|k_1\rangle|k_2\rangle \times e^{-i\tau(k_1-k_2)a_1^\dagger a_1}\left|\frac{\alpha}{\sqrt{2}}\right\rangle\!\!\right\rangle_{a_1} e^{i\tau(k_1-k_2)a_2^\dagger a_2}\left|\frac{\alpha}{\sqrt{2}}\right\rangle\!\!\right\rangle_{a_2}. \tag{16}$$

Using the fact that $e^{i\theta a^\dagger a}|\alpha\rangle = |e^{i\theta}\alpha\rangle$ we may evaluate the above to the form

$$|\psi(\tau)\rangle = e^{-|\alpha|^2/2}\sum_{k_1,k_2=0}^{N} \Psi_{k_1k_2}|k_1\rangle|k_2\rangle \times \exp\left[\frac{\alpha}{\sqrt{2}}\left(e^{-i\tau(k_1-k_2)}a_1^\dagger + e^{i\tau(k_1-k_2)}a_2^\dagger\right)\right]|\text{vac}\rangle. \tag{17}$$

The next step is to apply the beam splitter operation according to (7). The state then becomes

$$|\psi(\tau)\rangle = \sum_{k_1,k_2=0}^{N} \Psi_{k_1k_2}|k_1\rangle|k_2\rangle \times |\alpha\cos(k_1-k_2)\tau\rangle_c|-i\alpha\sin(k_1-k_2)\tau\rangle_d. \tag{18}$$

The last step is to detect the number of photons in each of the modes c, d. This is equivalent to the projection of the state (18) using the measurement operator

$$\Pi_{n_cn_d} = |n_c\rangle|n_d\rangle\langle n_c|\langle n_d|, \tag{19}$$

such that the final unnormalized state up to an irrelevant global phase is

$$\left|\widetilde{\psi}_{n_cn_d}(\tau)\right\rangle\!\!\right\rangle = \Pi_{n_cn_d}|\psi(\tau)\rangle \tag{20}$$
$$= |n_c\rangle|n_d\rangle \times \sum_{k_1,k_2=0}^{N} \Psi_{k_1k_2}C_{n_cn_d}[(k_1-k_2)\tau]|k_1\rangle|k_2\rangle, \tag{21}$$

where we defined the Fock state coefficients of a coherent state split with amplitudes $\cos\chi$ and $\sin\chi$ as (see Appendix A)

$$C_{n_c n_d}(\chi) \equiv \frac{\alpha^{n_c+n_d} e^{-|\alpha|^2/2}}{\sqrt{n_c! n_d!}} \cos^{n_c}\chi \sin^{n_d}\chi \tag{22}$$

which is normalized according to

$$\sum_{n_c,n_d=0}^{\infty} |C_{n_c n_d}(\chi)|^2 = 1. \tag{23}$$

The form (21) shows that the effect of the optical scheme is extremely simple — the initial wavefunction is modulated by an extra factor of $C_{n_c n_d}[(k_1-k_2)\tau]$. We shall explore the effect of this more in the next section.

The normalized state after measuring photons is given by

$$|\psi_{n_c n_d}(\tau)\rangle \equiv \frac{\left|\widetilde{\psi}_{n_c n_d}(\tau)\right\rangle}{\sqrt{p_{n_c n_d}(\tau)}}. \tag{24}$$

Here the normalization factor is equal to the photon detection probability

$$\begin{aligned} p_{n_c n_d}(\tau) &= \left\langle \widetilde{\psi}_{n_c n_d}(\tau) \middle| \widetilde{\psi}_{n_c n_d}(\tau) \right\rangle \\ &= \sum_{k_1,k_2=0}^{N} |\Psi_{k_1 k_2} C_{n_c n_d}[(k_1-k_2)\tau]|^2. \end{aligned} \tag{25}$$

For the initial state (13), after some algebra we can eliminate one of the summations to yield the equivalent expression

$$p_{n_c n_d}(\tau) = \frac{1}{4^N} \sum_{k=0}^{2N} \binom{2N}{k} |C_{n_c n_d}[(N-k)\tau]|^2. \tag{26}$$

From (23), one can see that the photon detection probability is normalized

$$\sum_{n_c,n_d=0}^{\infty} p_{n_c n_d}(\tau) = 1. \tag{27}$$

The state (24) is the desired entangled state of the two BECs. We analyze this state and the photon probability distribution (26) in the following sections.

III. APPROXIMATE STATE FOR SHORT TIMES

A. Analytic approximation of the state

We first consider short interaction times of the order $\tau \lesssim 1/\sqrt{N}$ between the light and the BECs. This regime will turn out to be the most relevant in terms of generating BEC-BEC entanglement, and it is also possible to make analytic approximations of the state. This will elucidate exactly what the nature of the entanglement generated between the BECs is.

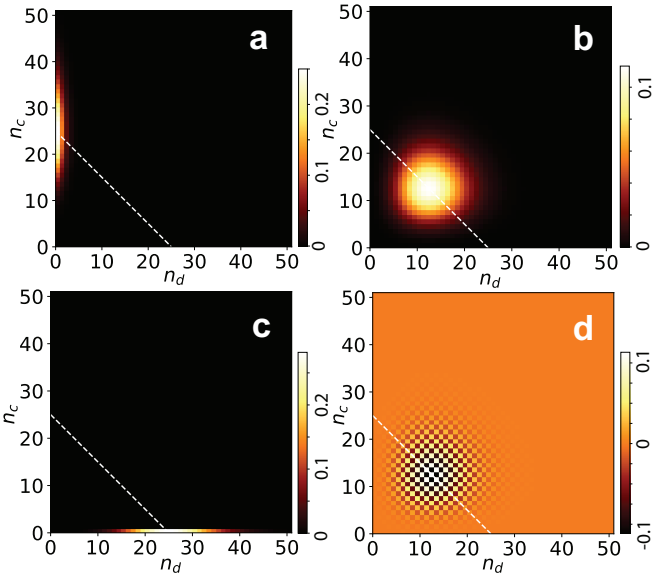

FIG. 2: The function $C_{n_c n_d}(\chi)$ defined in (22) for (a) $\chi = 0.1$; (b) $\chi = \pi/4$; (c) $\chi = \pi/2$; (d) $\chi = 5\pi/4$. All plots use $\alpha = 5$. The dashed line indicates the line $n_c + n_d = |\alpha|^2$, the dominant region where the coefficients have the largest magnitude.

First consider the dominant terms in (21) with the choice of initial state (13) with $N \gg 1$. Due to the binomial functions, only the terms in the range $N/2 - \sqrt{N} \lesssim k_1, k_2 \lesssim N/2 + \sqrt{N}$ have a significant coefficient. Thus for interaction times $\tau \lesssim 1/\sqrt{N}$, the argument of the $C_{n_c n_d}$ function, i.e. $(k_1 - k_2)\tau$, are all small since $|k_1 - k_2| \sim \sqrt{N}$. When $\chi \ll 1$ in (22), all terms except for $n_d = 0$ are small, due to the presence of the small factor $\sin\chi \ll 1$. Thus in the short time regime $\tau \lesssim 1/\sqrt{N}$, we may approximate

$$C_{n_c n_d}[(k_1-k_2)\tau] \approx \delta_{n_d=0} \frac{\alpha^{n_c} e^{-|\alpha|^2/2}}{\sqrt{n_c!}} \cos^{n_c}(k_1-k_2)\tau. \tag{28}$$

This may be directly observed in Fig. 2 where we plot the function $C_{n_c n_d=0}(\chi)$ for a variety of different χ. For $\chi \ll 1$ (see Fig. 2(a)) we observe that the only significant amplitudes occur for $n_d = 0$.

Now let us also consider that the BECs are illuminated by bright coherent light $|\alpha| \gg 1$. According to the distribution (28), a typical measurement outcome will be $n_c \sim |\alpha|^2, n_d = 0$. We may then approximate the cosine factor in (28) by a Gaussian distribution

$$\cos^{n_c}(k_1-k_2)\tau \approx e^{-\frac{n_c}{2}[(k_1-k_2)\tau]^2}. \tag{29}$$

We thus obtain an approximate expression for (21)

$$\left|\psi_{n_c}^{\text{approx}}(\tau)\right\rangle \propto \sum_{k_1,k_2=0}^{N} \Psi_{k_1k_2} e^{-n_c\tau^2(k_1-k_2)^2/2} \left|k_1\right\rangle \left|k_2\right\rangle \tag{30}$$

For the case that the initial state are polarized spin coherent states (13), the binomial factors in (21) can be also approximated by a Gaussian for $N \gg 1$

$$\frac{1}{2^N}\binom{N}{k} \approx \sqrt{\frac{2}{N\pi}} e^{-\frac{2}{N}(k-\frac{N}{2})^2}. \tag{31}$$

Using these we obtain an approximate expression for the wavefunction

$$\left|\psi_{n_c}^{\text{approx}}(\tau)\right\rangle = \frac{1}{\sqrt{\mathcal{N}}} \sum_{k_1,k_2=0}^{N} e^{-\frac{1}{N}\left[(k_1-\frac{N}{2})^2+(k_2-\frac{N}{2})^2\right]} \times e^{-n_c\tau^2(k_1-k_2)^2/2} \left|k_1\right\rangle \left|k_2\right\rangle, \tag{32}$$

which is valid for $N \gg 1$, $|\tau| \lesssim 1/\sqrt{N}$, $|\alpha| \gg 1$. Here, $\mathcal{N}$ is a normalization factor and can be approximated by (see Appendix B)

$$\begin{aligned}\mathcal{N} \approx & \vartheta_3(0, e^{-4/N})\vartheta_3(0, e^{-4(1/N+n_c\tau^2)}) \\ & + \vartheta_2(0, e^{-4/N})\vartheta_2(0, e^{-4(1/N+n_c\tau^2)}),\end{aligned} \tag{33}$$

where $\vartheta_n(z,q)$ is the Jacobi theta function.

The approximate wavefunction (32) clarifies the nature of the wavefunction created by the scheme shown in Sec. II. The first exponential term in (32) is a symmetric uncorrelated Gaussian in the Fock state distributions k_1, k_2. Meanwhile, the second exponential produces correlations in k_1, k_2, such that the coefficients of the states with $k_1 = k_2$ are most dominant in the sum.

In order to produce sharp correlations, (32) suggests that interaction times such that

$$\tau > \frac{1}{\sqrt{n_c}} \approx \frac{1}{|\alpha|} \tag{34}$$

should be chosen. This can be chosen consistent with the regime $\tau \lesssim 1/\sqrt{N}$ as long as

$$N < |\alpha|^2, \tag{35}$$

hence it is favorable to have bright coherent light for strong squeezing.

B. Analytic approximation of the photon probability

We can similarly obtain an approximate expression for the photon probability for $\tau \lesssim 1/\sqrt{N}$ and $N \gg 1$. Starting with (26) and we use the expression (28) and apply the Gaussian approximations (29) and (31). We obtain using similar methods to that in Appendix B

$$p_{n_cn_d}^{\text{approx}}(\tau) \propto \delta_{n_d=0} \frac{|\alpha|^{2n_c} e^{-|\alpha|^2}}{n_c!\sqrt{N\pi}} \vartheta_3(0, e^{-(1/N+n_c\tau^2)}), \tag{36}$$

which is valid for $N \gg 1$, $|\tau| \lesssim 1/\sqrt{N}$, $|\alpha| \gg 1$. Figure 3(a) shows the photon probability distribution for three interaction times. We see that in fact there is very little difference between the curves. The reason for this is that the n_c-dependence of the Jacobi theta function is very weak in (36). Assuming $\tau \sim 1/\sqrt{N}$, when $n_c > N$ the theta function approaches 1 and there is no n_c dependence. For $n_c < N$, due to the choice of α as given in (35), the photon probability is small and does not impact the shape the of the distribution. We can thus further approximate in this regime

$$p_{n_cn_d}^{\text{approx}}(\tau) \approx \delta_{n_d=0} \frac{|\alpha|^{2n_c} e^{-|\alpha|^2}}{n_c!}, \tag{37}$$

which is simply a Poisson distribution for the c-mode.

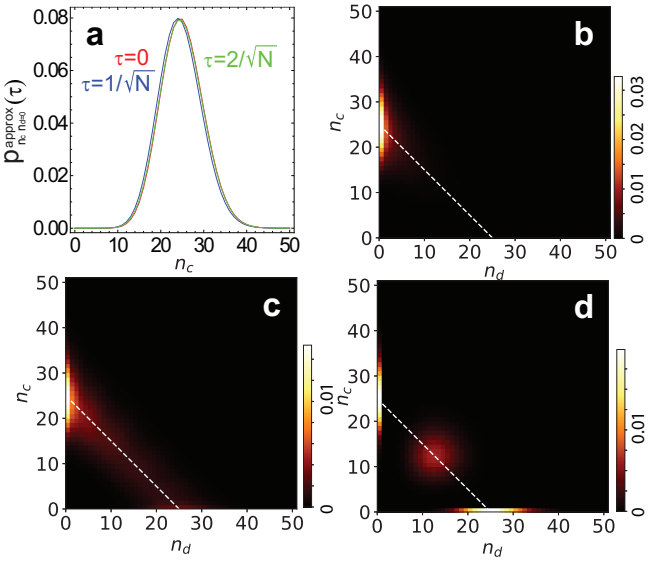

FIG. 3: Photon probability distribution. (a) Approximate probability distribution (36) for the interaction times as marked. (b)(c)(d) Exact probability distribution (26) for (b) $\tau = 0.1$; (c) $\tau = 0.23$; (d) $\tau = \pi/4$. All plots use parameters $N = 20$, $\alpha = 5$. The dashed line indicates the line $n_c + n_d = |\alpha|^2$, the dominant region where the coefficients have the largest magnitude.

C. Properties of the approximate state

In the limit of large $n_c\tau^2$, the approximate state (32) reduces to

$$\left|\psi_{\text{lim}}^{\text{approx}}\right\rangle \to \left(\frac{4}{\pi N}\right)^{1/4} \sum_{k=0}^{N} e^{-\frac{2}{N}(k-\frac{N}{2})^2} \left|k\right\rangle \left|k\right\rangle. \tag{38}$$

This is reminiscent of a maximally entangled spin-EPR state [66]

$$|\mathrm{EPR}\rangle = \frac{1}{\sqrt{N+1}} \sum_{k=0}^{N} |k\rangle\,|k\rangle\,, \tag{39}$$

except that there is a Gaussian amplitude weighting the wavefunction such that the amplitudes are larger nearer to the center $k = N/2$. The nature of the state (39) has been discussed in much detail elsewhere (see for example Ref. [66]). Due to the similar form of the state, we expect that the state (32) will have similar properties to the spin-EPR state. It is however useful to know what difference the Gaussian amplitude in (32) makes to the properties of the state. Thus here we give a short summary of the properties of the state (32), in particular examining the probability dsitributions, variance, and entanglement. This will give better intuition for understanding the nature of the unapproximated full wavefunction (21) studied in the next section.

1. *Spin probability distribution*

Let us first consider the probability distribution of measuring the state (32) in various bases. In addition to the eigenstates of S^z as given in (3), let us define the eigenstates of the S^x, S^y operators as

$$\begin{aligned} S^x|k\rangle^{(x)} &= (2k-N)|k\rangle^{(x)} \\ S^y|k\rangle^{(y)} &= (2k-N)|k\rangle^{(y)}. \end{aligned} \tag{40}$$

Explicit expressions for the eigenstates are given in Appendix C.

The probabilities of measuring the atoms in these basis are then given by

$$p_{\sigma_1\sigma_2}(k_1,k_2) = |\langle\Phi|\left(|k\rangle^{(\sigma_1)} \otimes |k\rangle^{(\sigma_2)}\right)|^2, \tag{41}$$

where in this case $|\Phi\rangle = |\psi_{n_c}^{\mathrm{approx}}(\tau)\rangle$. The probabilities for $\sigma_1 = \sigma_2$ are shown in Fig. 4(a)(b)(c). We compare the distribution to that generated by the two-axis two-spin (2A2S) squeezed state [66]

$$|\psi_{\mathrm{2A2S}}(\tau)\rangle = e^{-i(S_1^z S_2^x + S_1^x S_2^z)\tau}|\frac{\pi}{2},0\rangle\rangle|\frac{\pi}{2},0\rangle\rangle, \tag{42}$$

where we have rotated the basis such that correlations occur in the $S_{1,2}^z$ variables and anti-correlations in the $S_{1,2}^y$ variables. As discussed in Ref. [66], this produces a state that is approximately a spin-EPR state (39), for the optimal squeezing time. We calculate the probability distributions of the measurement (41), where $|\Phi\rangle = |\psi_{\mathrm{2A2S}}(\tau)\rangle$, the results are shown in Fig. 4(d)(e)(f).

First examining the probabilities in the S^z-basis (Fig. 4(c)(f)), we see that strong correlations are formed thanks to the Gaussian squeezing factor in (32). Only the terms with $k_1 = k_2$ have high probabilities, showing correlations. The main difference to the 2A2S squeezed state

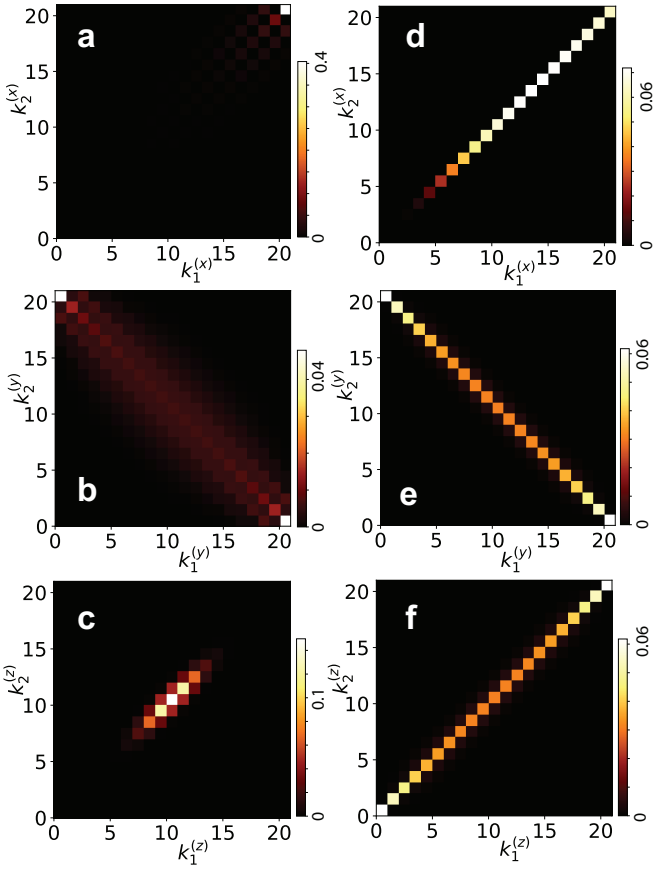

FIG. 4: Probability distribution for measurements of the state (a)(b)(c) $|\psi_{n_c}^{\mathrm{approx}}(\tau)\rangle$ given in (32) for $N = 20$, $n_c\tau^2 = 0.23\sqrt{20}$ and (d)(e)(f) the 2A2S state given in (42) for $N = 20$, $\tau = 2/N$. Measurements are made in the eigenstates of the (a)(d) S^x; (b)(e) S^y; (c)(f) S^z operators.

here is that the distribution along $k_1 = k_2$ are weighted by a Gaussian factor, such that only Fock states with $N/2 - \sqrt{N} \lesssim k_1, k_2 \lesssim N/2 + \sqrt{N}$ have a significant probability. In contrast, the 2A2S squeezed state has a more even amplitude distribution.

For the probabilities in the S^y-basis (Fig. 4(b)(e)), we see that the main probabilities occur along $k_1 = N - k_2$, displaying anti-correlations. The anti-correlations in (32) are considerably broader along the anti-diagonal in comparison to the 2A2S squeezed state. This can be attributed to the Gaussian factor which modulates the amplitude in the S^z correlations. Similar to a Fourier transformation, the broader the distribution for the S^z correlations, the sharper the anti-correlations in the S^y variables.

Finally, for the probabilities in the S^x-basis (Fig. 4(a)(d)), a twin-Fock state like distribution is produced for both (32) and the 2A2S squeezed state. Due to the initial state being S^x-polarized states, the highest weight is for $k_1^{(x)} = k_2^{(x)} = N$, with addition terms in the superposition being generated by the effective interaction.

In summary, the approximate state (32) produced by

the optical protocol has the same correlations and anti-correlations as that produced by the 2A2S squeezed state (42), which in turn is similar to the spin-EPR state (39). The main difference is in the amplitude dependence in the S^z-basis measurements, originating from the first Gaussian factor in (32). This produces broader anti-correlations in the S^y-basis measurements.

2. *Variances and expectation values*

From the probability distributions examined in the last section, we expect that particular spin combinations will attain low values of the variance. From the distributions in Fig. 4, we expect that the variances of the combinations $S_1^x - S_2^x, S_1^y + S_2^y, S_1^z - S_2^z$ should remain small. For the 2A2S squeezed state (42), the variance of the $S_1^x - S_2^x$ is zero for all time, while the variance of $S_1^y + S_2^y$ and $S_1^z - S_2^z$ decay with exactly the same time-dependence [66].

In Fig. 5(a) we calculate the variances of the three operators pairings for the approximate state (32). For the $S_1^z - S_2^z$ variance, we see that this approaches zero in a similar way to the 2A2S squeezed state. However, the $S_1^y + S_2^y$ variance does not completely decay to zero and saturates to a value N. We attribute this to the broader anti-correlations that are produced, as seen in Fig. 4(b). Meanwhile, the $S_1^x - S_2^x$ variance increases and converges to a value N. The variance of this quantity initially starts at zero because the initial state are S^x-polarized states. This is unlike the 2A2S squeezed state where the variance is zero for all time due to the twin-Fock nature of the state. Here again the correlations are broader and occur along the off-diagonal elements in Fig. 4(a).

The spin expectation values for the approximate state (32) are plotted in Fig. 6(a). In this case, the dependence more resembles the 2A2S squeezed state, where the initially polarized spins in the S^x-direction decay to zero. The other spin expectation values are zero for all time, similarly to the 2A2S squeezed state.

3. *Entanglement*

We finally examine the entanglement in the state (32). This can be quantified for the pure state using the von Neumann entropy

$$E(\rho) = -\operatorname{Tr}(\rho \log_2 \rho), \tag{43}$$

where

$$\rho = \operatorname{Tr}_2(|\psi_{n_c}^{\text{approx}}(\tau)\rangle\langle\psi_{n_c}^{\text{approx}}(\tau)|) \tag{44}$$

is the reduced density matrix on BEC 1. Here Tr_2 is the partial trace over the states in BEC 2.

In Fig. 7(a) we show the entanglement as a function of $n_c\tau^2$ for state (32). As expected the amount of entanglement increases monotonically with the amount of correlations that are generated. The entanglement increases

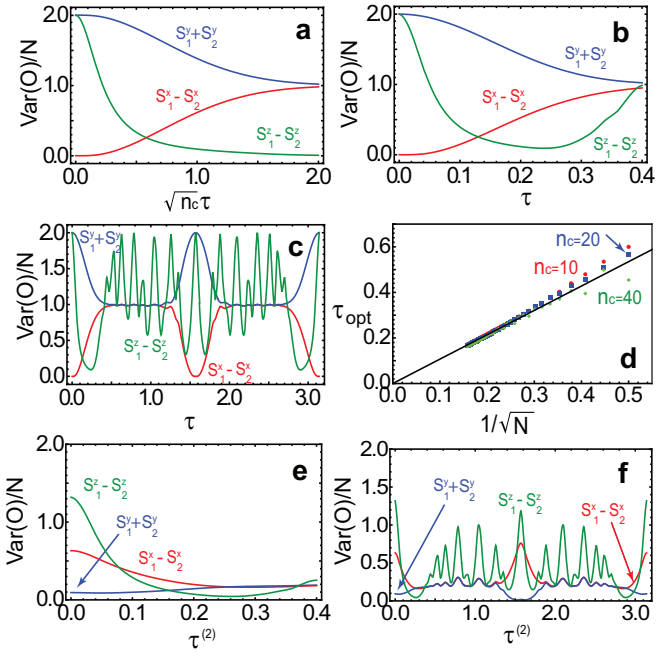

FIG. 5: Variances of the two-spin squeezed state for the operators $\mathcal{O}$ as marked, using the (a) approximate state (32); (b) exact state (24) for short time scales; (c) exact state (24) for long time scales; (e) the 2 pulse scheme (56) for short time scales; (f) the 2 pulse scheme (56 for long time scales. For the one pulse state we choose parameters $N = 20$, $n_c = 20$, $n_d = 0$ in (a)(b)(c). For the two pulse state choose $N = 20$, $n_c^{(1)} = n_c^{(2)} = 20$, $n_d^{(1)} = n_d^{(2)} = 0$, $\tau^{(1)} = 0.23 \approx \tau_{\text{opt}}$, and $\tau^{(2)} = \tau$ in (e)(f). (d) The optimal squeezing time τ determined by minimizing $\Delta^2(S_1^z - S_2^z)$ as a function of N. We choose parameters $n_d = 0$ and n_c as marked.

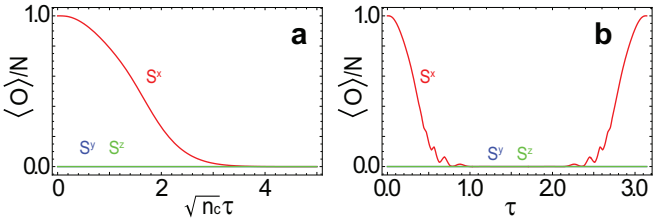

FIG. 6: Expectation values of the two-spin squeezed state for the operators $\mathcal{O}$ as marked. Expectation values using the (a) approximate state (32); (b) exact state (24). We choose parameters $N = 20$, $n_c = 20$, $n_d = 0$ throughout.

and saturates towards a limiting value E_{lim}. The limiting value can be deduced by finding the reduced density matrix for (38), which is already in diagonal form

$$\rho_{\text{lim}} = \sqrt{\frac{4}{\pi N}} \sum_{k=0}^{N} e^{-\frac{2}{N}(k-\frac{N}{2})^2} |k\rangle\langle k|. \tag{45}$$

Evaluating the entanglement for this state we obtain for

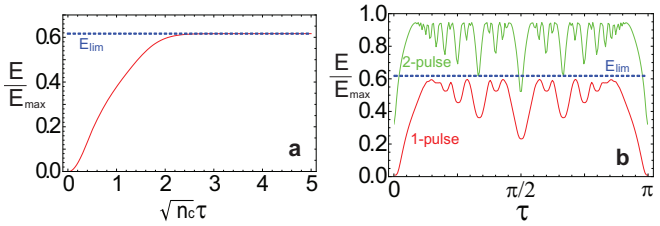

FIG. 7: Entanglement produced between two BECs using the optical protocol. The von Neumann entropy for (a) the approximate state (32) for $N = 20$; (b) the exact state (24) for parameters $N = 20$, $n_c = 20$, $n_d = 0$ and the two-pulse state (56) for parameters $N = 50$, $n_c^{(1)} = n_c^{(2)} = 50$, $n_d^{(1)} = n_d^{(2)} = 0$, $\tau^{(1)} = 0.1$, and $\tau^{(1)} = \tau$ as plotted in the figure.

$N \gg 1$

$$E_{\rm lim} \approx \frac{1}{2}\log_2 \frac{N\pi e}{4} \approx \frac{1}{2}\log_2 N + 0.547. \qquad (46)$$

Since maximum entanglement that can be reached between two $N+1$ dimensional systems is

$$E_{\rm max} = \log_2(N+1), \qquad (47)$$

we see that for large systems the amount of entanglement that can be generated is

$$\lim_{N\to\infty} \frac{E_{\rm lim}}{E_{\rm max}} = \frac{1}{2}. \qquad (48)$$

We see that due to the Gaussian factors, the entanglement that can be generated using the optical scheme is less than the maximum. However, it is still a macroscopic amount of entanglement, of is of the same order as the maximal entanglement. We shall see how this can be further improved in Sec. V.

IV. NUMERICAL ANALYSIS OF THE ENTANGLED STATE

In this section we analyze the state (24) and photon probability distribution (26) using a numerical approach. This will allow us to confirm the behavior at short interaction times as investigated in the previous section, and examine the behavior at longer times.

A. Photon probability distribution

Figure 3(b)(c)(d) shows the photon probability using the exact distribution (26) for several different interaction times. For short interaction times (Fig. 3(b)) we see that the photons are almost completely in mode c, with a Poissonian distribution as discussed in Sec. III B. We can understand this also from the perspective of Fig. 1. In the Mach-Zehnder configuration of the light, when the light is relatively unperturbed due to the small interaction, constructive interference will occur for mode c and destructive interference for mode d.

For longer interaction times (Fig. 3(c)(d)), photons start to emerge with outcomes $n_d > 0$. The dominant regions where the photons energy are along the line $n_c + n_d = |\alpha|^2$, since the number of photons is conserved by the Hamiltonian. To understand the nature of the broadening, first consider the behavior of the $C_{n_c n_d}(\chi)$ function as plotted in Fig. 2. Due to this function being the amplitude of a coherent state split by a beam splitter (see Appendix A), the typical outcome occurs at $n_c \sim |\alpha|^2 \cos^2\chi$ and $n_d \sim |\alpha|^2 \sin^2\chi$. Now for $N \gg 1$ we can approximate the binomial function by a Gaussian using (31), giving

$$p_{n_c n_d}(\tau) \approx \frac{1}{\sqrt{N\pi}} \sum_{k=-\infty}^{\infty} e^{-k^2/N} |C_{n_c n_d}(k\tau)|^2. \qquad (49)$$

This is a convolution of the beam split photon probabilities with a Gaussian. The dominant terms in the sum are those with $-\sqrt{N}\tau \lesssim k\tau \lesssim \sqrt{N}\tau$, which causes the broadening seen in Fig. 3(c). For Fig. 3(d), there are three dominant peaks because in this case $k\tau = k\pi/4$, the peaks occur at the three angles $\chi = 0, \pi/4, \pi/2$. This is similar to the resonances observed in one-axis two-spin sqeezed states [64].

B. Spin probability distribution

We now examine the spin probability distributions (41) for the exact state (24). In Fig. 8 we plot all 9 spin combinations of σ_1, σ_2. Comparing the corresponding approximated distributions in Fig. 4, the three diagonal distributions $\sigma_1 = \sigma_2$ visually are identical, with the same pattern of correlations and anti-correlations. The same broadening of the (S_1^y, S_2^y) distributions are also seen here with the exact wavefunction. As explained in Sec. III C 1, this is due to the Gaussian envelope of the S_1^z, S_2^z distribution.

For the other off-diagonal spin combinations $\sigma_1 \neq \sigma_2$, we see distributions which are symmetrical on one of the variables, which gives rise to zero correlations. The pattern of the distribution has a resemblance to the two-axis two-spin squeezed states, with semicircular features emerging (see Fig. 4 of Ref. [66]). We note that off-diagonal spin combinations $\sigma_1 \neq \sigma_2$ of the approximate wavefunction (32) are visually identical (not plotted) to the probability distribution using the exact wavefunction (24) for these parameters. The strong similarity of the distributions in Fig. 4 and Fig. 8 show that the wavefunction (32) is an excellent approximation to the exact (24).

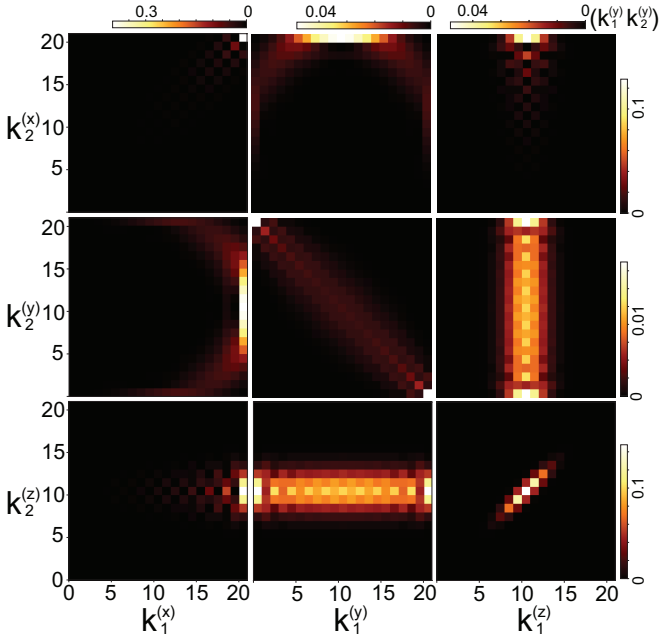

FIG. 8: Probability distribution after measuring the state (24) in various bases according to (41) on the two BECs. We use parameters $N = 20$, $n_c = 20$, $n_d = 0$, $\tau = 0.23 \approx \tau_{\rm opt}$, close to the optimally squeezed time. The density plot legends for similar shaped distributions are the same. The legend for the S_1^y, S_2^y is shown top right.

C. Variances and expectation values

The variances of three correlated and anti-correlated spin pairs are shown in Fig. 5(b)(c). At short time scales (Fig. 5(b)), the variances of $S_1^x - S_2^x$ and $S_1^y + S_2^y$ of the exact state (24) are nearly identical to that of the approximate state (32) as shown in Fig. 5(a). Both of these quantities approach N and remain at this value for some time (Fig. 5(c)), until revivals are seen at times $\tau = k\pi/2$, for integer k. The interaction time τ is periodic in units of π for all quantities.

For the variable $S_1^z - S_2^z$, which exhibits the largest amount of squeezing, the dependence agrees well with the short-time approximation for times $\tau \lesssim 1/\sqrt{N}$ as can be seen by comparing Fig. 5(a) and 5(b). After these times the approximation breaks down and the variance starts to increase (Fig. 5(b)). There is thus an optimal interaction time $\tau_{\rm opt}$ where the squeezing is optimized, in a similar way to the two-axis two-spin state [66]. At longer time scales (Fig. 5(c)), the variance shows some complex oscillatory behavior, but does return to the same variance until a time $\tau = \pi - \tau_{\rm opt}$, which occurs due to the periodicity of the interaction.

Figure 5(d) shows the optimal sqeezing time, obtained by minimizing the variance of $S_1^z - S_2^z$, as a function of N for various choices of n_c and $n_d = 0$. Despite the scaling with $\sqrt{n_c}$ as suggested in Fig. 5(a), we observe that for the optimal time there is little dependence on n_c. We attribute this to the fact that the $\sqrt{n_c}$ scaling is derived in Sec. III B for short times $\tau \lesssim 1/\sqrt{N}$, and the optimal squeezing time is on the edge of the validity of this regime. The optimal squeezing time is found to show a scaling behavior agreeing very well for large N with the relation

$$\tau_{\rm opt} \approx \frac{1.07}{\sqrt{N}}. \tag{50}$$

For the expectation values, the agreement between the approximate wavefunction (Fig. 6(a)) and exact wavefunction (Fig. 6(b)) generally shows excellent agreement. The expectation values of S^y and S^z are zero for all time, and S^x shows a Gaussian decay as seen before. The exact wavefunction shows a revival of the S^x expectation value at a time $\tau = \pi$, due to the periodicity of the exact wavefunction. The approximate wavefunction does not capture this long time behavior.

D. Entanglement

In Fig. 7(b) we plot the von Neumann entropy as a function of interaction time τ for the exact state (24). We see that for short times $\tau \lesssim 1/\sqrt{N}$ the behavior of the entanglement agrees well with the approximate state as shown in Fig. 7(a). After these times, the curve shows a typical "devil's crevasse" dependence as observed in Ref. [64], where entanglement fluctuates in a fractal pattern depending on whether the interaction time is a rational multiple of π. This behavior occurs due to the similar nature of interaction that was considered both in Ref. [64] and this work, which are both a $S_1^z S_2^z$ type Hamiltonian. The pattern repeats with a period of π due to the periodicity of the wavefunction. We note that for the longer interaction times, photonic outcomes with $n_d > 0$ become more probable. Hence Fig. 7(b) would represent the case where only the $n_d = 0$ is considered, and other cases show a different dependence. This is in contrast to the short-time regime where the $n_d = 0$ case is the most probable outcome.

As discussed in Sec. III C 3, there is a ceiling to the entanglement that can be generated, which agrees well with the limiting value of entanglement (46). This occurs due to the Gaussian amplitude of the initial state, and was also observed in Ref. [64].

E. Correlation based entanglement and EPR steering detection

Figure 7 shows that entanglement is present between the BECs at all times except $\tau = n\pi$, where n is an integer. Calculating the von Neumann entropy requires finding the eigenvalues of the reduced density matrix, which is difficult to extract experimentally in high dimensional systems due to the large number of measurements required. It is therefore more desirable to have

entanglement criteria that are based on low-order correlations of spin operators, which are more viable to obtain in an experimental context. A comparative study of various criteria was performed in Ref. [66] for the two-axis two-spin squeezed state, which has similarities to the state that we consider here. It was found there that the Hofmann-Takeuchi criterion [79]

$$\mathcal{C}_{\rm ent} \equiv \frac{{\rm Var}(S_1^x - S_2^x) + {\rm Var}(S_1^y + S_2^y) + {\rm Var}(S_1^z - S_2^z)}{4N} \geq 1, \tag{51}$$

which holds for any separable state, was most suitable for detecting this type of entangled state. The reason for the success of this criterion stems from the fact that it does not involve a comparison with any expectation values of spins $\langle S^x\rangle, \langle S^y\rangle, \langle S^z\rangle$, which all decay to zero as seen in Fig. 6.

Figure 9(a) shows the left hand side of the criterion (51) for the exact state (24). We find that entanglement is detected for some times except for times $\tau = n\pi/2$. There are some times where the violation of (51) is extremely small, such as $\tau = \pi/4$. Comparison with Fig. 7(b) shows that these times such as $\tau = \pi/2$ are in fact entangled, but the criterion only just detects entanglement. The fact that the Hofmann-Takeuchi criterion is able to detect entanglement for the full range of times is rather remarkable, since for other similar states such as the 1A2S [61, 64] and 2A2S squeezed states [66], entanglement is only successfully detected for a limited range of times.

EPR steering can similarly be detected using a correlation based criterion. The criterion developed by Reid and co-workers [54, 61, 80] states that EPR steering from BEC 1 to BEC 2 is present if it violates the inequality

$$\mathcal{C}^{1\to 2}_{\rm steer} \equiv \frac{{\rm Var}(S_1^y + S_2^y){\rm Var}(S_1^z - S_2^z)}{\langle S_1^x\rangle^2} \geq 1. \tag{52}$$

Figure 9(b) shows that EPR steering is detected in the short time range. The largest violation is seen around $\tau_{\rm opt}$, which is the time when the largest squeezing is observed. The fact that EPR steering is detected in a smaller range than entanglement is consistent with the notion that EPR steering is a quantity that is higher in the hierarchy of quantum correlations [81, 82]. We note that although EPR steering is generally an asymmetric property, in our case it is symmetric as the state is symmetric with respect to interchange of BECs 1 and 2.

F. Bell-CHSH correlations

One of the interesting features of the two-axis two-spin squeezed state (42) is that it violates a Bell-CHSH inequality for all N [66]. Due to the similarity of the state generated using our scheme, we can reasonably expect that Bell-CHSH correlations may be present in our state. The Bell-CHSH inequality [83] for two observers with two

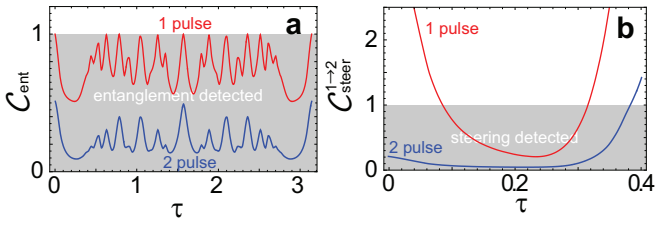

FIG. 9: Detection of entanglement and EPR steering using correlation based criteria. (a) The Hofmann-Takeuchi criterion (51) for the exact state (24) and the two-pulse state (56). (b) The EPR steering detection criterion (52) for the exact state (24) and the two-pulse state (56). For the state (24) we use parameters $N = 20$, $n_c = 20$, $n_d = 0$; for the state (56) we use the parameters $N = 20$, $n_c^{(1)} = n_c^{(2)} = 20$, $n_d^{(1)} = n_d^{(2)} = 0$ and choose the first interaction time to be $\tau^{(1)} = 0.23 \approx \tau_{\rm opt}$. For the two-pulse scheme the interaction time refers to the second pulse time $\tau = \tau^{(2)}$.

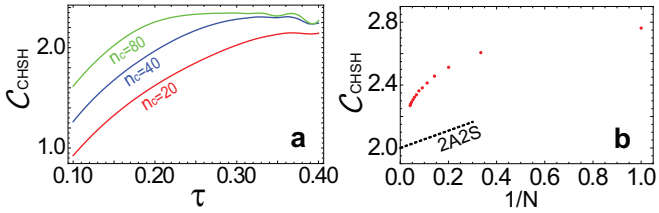

FIG. 10: Bell-CHSH correlations in the state (24). (a) Time dependence of (53) for various choices of n_c as marked. We use parameters $\theta_B = 0.2$, $N = 15$, $n_d = 0$. (b) Optimized values of (53) with respect to τ and θ_B for various N. We choose parameters $n_c = 4N$, $n_d = 0$. The dotted line shows (53) for the case of the two-axis two-spin (2A2S) squeezed state (see Eq. (60) from Ref. [66]).

local measurement choices states that every local realist theory satisfies

$$\mathcal{C}_{\rm CHSH} = \Big|\langle M_1^{(1)} M_2^{(1)}\rangle + \langle M_1^{(1)} M_2^{(2)}\rangle - \langle M_1^{(2)} M_2^{(1)}\rangle + \langle M_1^{(2)} M_2^{(2)}\rangle\Big| \leq 2, \tag{53}$$

where $M_1^{(i)}, M_2^{(j)}$ are local, two-outcome measurement choices on BEC 1 and BEC 2 respectively, and $i, j \in \{1, 2\}$ label the two measurement choices. We use the same strategy as that given in Ref. [66], where the measurement operators are chosen to be

$$\begin{aligned} M_1^{(1)} &= {\rm sgn}(S_1^z) \\ M_1^{(2)} &= {\rm sgn}(S_1^z \cos\theta + S_1^y \sin\theta_B) \\ M_2^{(1)} &= {\rm sgn}(S_2^z \cos\frac{\theta_B}{2} + S_2^y \sin\frac{\theta_B}{2}) \\ M_2^{(2)} &= {\rm sgn}(S_2^z \cos\frac{\theta_B}{2} - S_2^y \sin\frac{\theta_B}{2}). \end{aligned} \tag{54}$$

While other choices of measurement operators may lead to stronger violations, the above choice has the advantage that it is experimentally viable since it is relatively

insensitive to errors at the single atom level. In contrast, parity measurements are very sensitive to experimental errors since an error at the single atom level reverses the measurement outcome [84].

The two parameters θ and τ should be optimized such that a maximal violation of (53) is obtained for each choice of N and n_c, n_d. We again focus on the short time region such that we take $n_d = 0$ to be the most likely outcome. Figure 10(a) shows the time dependence of the left hand side of the criterion (53) for the state (24) for various choice of n_c. For large values of n_c, the largest violation occurs at times $\approx \tau_{\rm opt}$. Larger violation tend to be found for larger values of n_c, which we attribute to higher level of squeezing being attained for larger n_c. For θ_B, we numerically find that the optimal angles follow a relation

$$\theta_B \approx \frac{3.2/N + 1.7/N^2}{1 + 2.1/N}, \tag{55}$$

where we used a Padé approximant to fit the data.

In Fig. 10(b) we show the optimized value of (53) as a function of N. We choose a photon number n_c that increases in proportion to N, such as a to satisfy (35). We observe that violations occur for all N, but the amount of violation decreases as the system size is increased. The decrease in the amount of violation was also observed in the case of two-axis two-spin squeezed states, also shown in Fig. 10(b) for comparison. Surprisingly, the amount of violation is much larger in our case despite the fact that our state is less than the ideal spin-EPR state (III C) due to the Gaussian amplitude factors present in the state. The CHSH correlators $\mathcal{C}_{\rm CHSH}$ appear to approach the classical value value of 2 in the limit of large N. Thus again for this state Bell violations appear to be present for all N, although the detection may be challenging for large ensembles.

V. TWO-PULSE SCHEME

A. The wavefunction

The probability distribution of correlations and anti-correlations shown in Fig. 4 suggests that there may be a way to improve the correlations further such that it further approaches the ideal spin-EPR state (39). As discussed in Sec. III C 2, the reason for the larger value of the variance of $S_1^y + S_2^y$ is the broader anti-correlations in the (S_1^y, S_2^y) amplitudes as seen in Fig. 8. From the analysis in Sec. III A, we found that in the short time limit $\tau \lesssim 1/\sqrt{N}$, the effect of the interaction was to suppress the off-diagonal amplitudes $k_1 \neq k_2$ with a Gaussian distribution. This means that after obtaining (24) with the first pulse, then performing a suitable basis rotation such that the (S_1^y, S_2^y) anti-correlations are turned into (S_1^z, S_2^z) correlations, we should be able to further squeeze the state.

The two pulse scheme then proceeds as follows. Starting from (24), we apply the transformation $e^{iS_1^x\pi/4}e^{-iS_2^x\pi/4}$ which transforms $S_1^y \to S_1^z$ and $S_2^y \to -S_2^z$. Then a second optical pulse is applied with the same protocol, where the light interaction for a duration $\tau^{(2)}$, and measurement outcomes $n_c^{(2)}, n_d^{(2)}$. Performing similar steps to that shown in Sec. II B, we obtain the final two-pulse wavefunction

$$\begin{aligned}|\psi_{n_c^{(1)}n_d^{(1)}n_c^{(2)}n_d^{(2)}}(\tau^{(1)},\tau^{(2)})\rangle &= \frac{1}{\sqrt{\mathcal{N}_2}}\sum_{k_1,k_2,k_1',k_2'=0}^{N} \\ &\times \sqrt{\binom{N}{k_1'}\binom{N}{k_2'}}\langle k_1|e^{iS^x\pi/4}|k_1'\rangle\langle k_2|e^{-iS^x\pi/4}|k_2'\rangle \\ &\times C_{n_c^{(1)}n_d^{(1)}}[(k_1'-k_2')\tau^{(1)}]C_{n_c^{(2)}n_d^{(2)}}[(k_1-k_2)\tau^{(2)}]|k_1\rangle|k_2\rangle\end{aligned} \tag{56}$$

where $\mathcal{N}_2$ is a normalization factor, and the matrix elements of $e^{-iS^x\theta/2}$ are given in (C3). Here, in the two-pulse protocol we label quantities relating to the first pulse with a $^{(1)}$, such that the $\tau^{(1)}$ is the interaction time and $n_c^{(1)}, n_d^{(1)}$ are the measurement outcomes of the first pulse.

The probability distribution for (56) is shown in Fig. 11 for all measurement combinations as defined in (41). In comparison to the distributions of the one-pulse state as shown in Fig. 8, we see a marked improvement of the pattern of correlations and anti-correlations. In particular the (S_1^y, S_2^y) distribution shows a much clearer anti-correlation. Also the (S_1^z, S_2^z) distribution suffers to a lesser extent from the Gaussian amplitude distribution which was limiting the value of the correlations.

Variances of spin operators as a function of interaction time are shown in Fig.5(e)(f). At shorter timescales (Fig.5(e)), we see that the two-pulse scheme manages to obtain much better values for the fluctuations which go very near zero for all three variables, as expected from the probability distribution plots. For longer timescales (Fig.5(f)), the variances show some oscillatory behavior, but overall the variance remains lower than the one-pulse scheme as can be seen in Fig. 5(c).

In Fig. 7(b) we plot the entanglement generated by the two-pulse scheme, as a function of the second pulse interaction time $\tau^{(2)}$. The overall shape is similar to the one-pulse scheme, but there are two important differences. Firstly, for $\tau^{(2)} = 0$ the entanglement is not zero, since the first pulse time is chosen to be $\tau^{(1)} \approx \tau_{\rm opt}$, such that entanglement is present. Moreover, the maximum entanglement is much larger in this case with a ceiling in the region of $E_{\rm lim}^{(2)} \approx 0.95 E_{\rm max}$. Thus the two-pulse scheme can improve the entanglement considerably, and approaches to a much better extent the maximally entangled state (39).

Correlation based detection of entanglement and EPR steering is also greatly improved with the two-pulse scheme. In Fig. 9(a) the Hofmann-Takeuchi criterion (51) is plotted for the two-pulse state (56). We see that

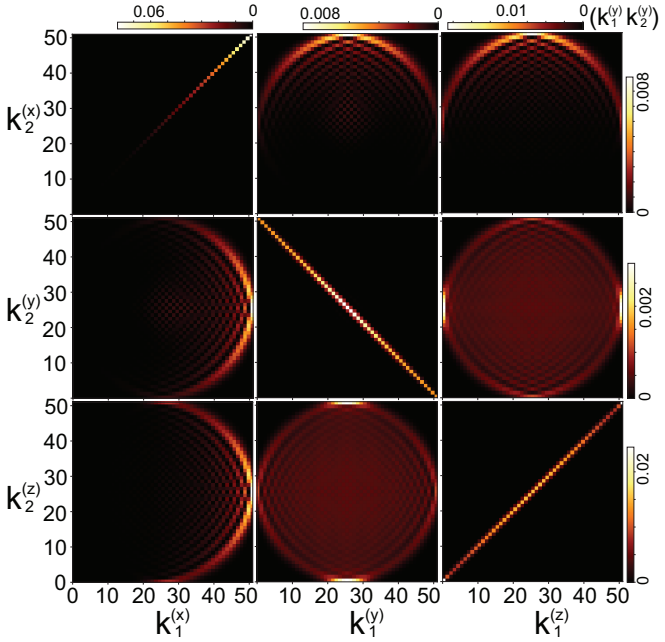

FIG. 11: Probability distribution after measuring the state (56) in various bases according to (41) on the two BECs. We use parameters $N = 50$, $n_c^{(1)} = n_c^{(2)} = 50$, $n_d^{(1)} = n_d^{(2)} = 0$, $\tau^{(1)} = \tau^{(2)} = 0.1 \approx \tau_{\rm opt}$, close to the optimally squeezed time. The density plot legends for similar shaped distributions are the same. The legend for the S_1^y, S_2^y is shown top right.

entanglement is detected for all times, and the violations are much stronger. The same is true for the EPR steering, shown in Fig. 9(b). The steering inequality shows violations that are much stronger, particularly for both pulses tuned to the optimal times $\tau_{\rm opt}$.

VI. SUMMARY AND CONCLUSIONS

We have analyzed a scheme for producing two-spin squeezed states of two spinor BECs. The final state that is produced is given by (24), but is very well approximated by (32) in the short time regime $\tau \lesssim 1/\sqrt{N}$. Since the optimal squeezing occurs at times $\tau_{\rm opt} \sim 1/\sqrt{N}$ the approximate wavefunction captures the primary region of interest. The technique involves interfering coherent light in a Mach-Zehnder configuration, which interacts with the two BECs. Performing a photon number measurement projects entanglement onto the two BECs. The quantum measurement thus randomly affects the wavefunction depending on the outcomes n_c, n_d. While strictly speaking this means that our protocol is nondeterministic, in the short time regime, the most likely outcome is $n_d = 0$ and the random fluctuations only occur in n_c according to (37). Since the effect of n_c in (32) is only to affect the degree of squeezing, the nature of the state is not dramatically affected by the randomness of the measurements.

The basic effect of the scheme in the short time limit can be understood very simply by inspecting (30): Fock state amplitudes with unequal eigenvalues with respect to S_1^z, S_2^z are suppressed with a Gaussian envelope. In this work we considered an initial state consisting of an S^x polarized state for both BECs, since this is a state that can be produced relatively simply. Since spin coherent states have amplitudes involving a binomial distribution, the culprit of the imperfect entanglement is due to this initial state. However, this can be remedied to a great extent by applying the protocol twice, where a local basis transformation is made such as to rotate $S_1^y \to S_1^z$ and $S_2^y \to -S_2^z$. This sequence produces greatly improves most aspects of the state such as the level of squeezing and entanglement.

One of the most attractive aspects of the current scheme is that it has a highly flexible geometry that allows for BECs to be entangled with two completely separate light beams. Similar schemes have been considered in past works before [52, 85] but generally the optical pulse must pass through each BEC sequentially. The Mach-Zehnder configuration allows for highly separated BECs to be entangled even when the line-of-sight is obstructed. The entanglement that is generated is potentially useful for quantum information applications such as quantum computing [67, 68] and quantum teleportation [86, 87], where it can be used as a quantum gate to produce entangled states.

Another interesting aspect of the states that are produced are that they are able to violate a Bell-CHSH inequality. The type of measurement that is required is relatively insensitive to single atom number fluctuations, since it involves the sign of spin operators. The level of violation is larger than that produced in two-axis two-spin states after optimizing the interaction time and Bell angles for both cases. However the amount of Bell violation decreases with atom number, as is the case with two-axis two-spin squeezed states, which make them potentially difficult to observe for large atom ensembles. Using a larger number of measurement settings and measurement outcome it may be possible to improve upon the level of violation without resorting to observables that are highly sensitive to single atom fluctuations, such as parity measurements.

Acknowledgments

This work is supported by the Shanghai Research Challenge Fund; New York University Global Seed Grants for Collaborative Research; National Natural Science Foundation of China (61571301,D1210036A); the NSFC Research Fund for International Young Scientists (11650110425,11850410426); NYU-ECNU Institute of Physics at NYU Shanghai; the Science and Technology Commission of Shanghai Municipality (17ZR1443600,19XD1423000); the China Science and Technology Exchange Center (NGA-16-001); and the

NSFC-RFBR Collaborative grant (81811530112). IS and LR thank the DAAD RISE Worldwide program for their support.

[1] H. Takahasi, in *Advances in Communication Systems* (Elsevier, 1965), vol. 1, pp. 227–310.
[2] D. W. Robinson, Communications in Mathematical Physics **1**, 159 (1965).
[3] D. Stoler, Physical Review D **1**, 1925 (1970).
[4] D. F. Walls, Nature **306**, 141 (1983), ISSN 00280836.
[5] M. O. Scully and M. S. Zubairy, *Quantum optics* (1999).
[6] C. Gerry, P. Knight, and P. L. Knight, *Introductory quantum optics* (Cambridge university press, 2005).
[7] D. F. Walls and G. J. Milburn, *Quantum optics* (Springer Science & Business Media, 2007).
[8] S. Machida and Y. Yamamoto, Physical Review Letters **58**, 1000 (1987).
[9] R. M. Shelby, M. D. Levenson, S. H. Perlmutter, R. G. Devoe, and D. F. Walls, Physical Review Letters **57**, 691 (1986), ISSN 00319007.
[10] R. E. Slusher, L. W. Hollberg, B. Yurke, J. C. Mertz, and J. F. Valley, Physical Review Letters **55**, 2409 (1985), ISSN 00319007.
[11] L.-A. Wu, H. J. Kimble, J. L. Hall, and H. Wu, Physical Review Letters **57**, 2520 (1986).
[12] M. Schwarzhans, L. Rauch, and M. J. J. Weimerkirch, Nature **387**, 471 (1997).
[13] R. S. Bondurant and J. H. Shapiro, Physical Review D **30**, 2548 (1984).
[14] E. Giacobino, C. Fabre, and G. Leuchs, Physics World **2**, 31 (1989), ISSN 0953-8585.
[15] R. E. Slusher and B. Yurke, Journal of Lightwave Technology **8**, 466 (1990), ISSN 15582213.
[16] M. Hillery, Physical Review A **61**, 022309 (2000).
[17] J. P. Dowling, Contemporary physics **49**, 125 (2008).
[18] R. Schnabel, Physics Reports **684**, 1 (2017).
[19] J. D. Macomber and R. Lynch, The Journal of Chemical Physics **83**, 6514 (1985), ISSN 00219606.
[20] D. F. Walls and P. Zoller, Physical Review Letters **47**, 709 (1981), ISSN 00319007.
[21] K. Wodkiewicz and J. H. Eberly, Journal of the Optical Society of America B **2**, 458 (1985), ISSN 0740-3224.
[22] D. J. Wineland, J. J. Bollinger, W. M. Itano, F. L. Moore, and D. J. Heinzen, Physical Review A **46**, R6797 (1992), ISSN 1050-2947.
[23] L. Vernac, M. Pinard, and E. Giacobino, Physical Review A **62**, 063812 (2000).
[24] C. Gross, Journal of Physics B: Atomic, Molecular and Optical Physics **45**, 103001 (2012).
[25] Z. Zhang and L. M. Duan, New Journal of Physics **16**, 103037 (2014).
[26] M. Kitagawa and M. Ueda, Physical Review A **47**, 5138 (1993).
[27] A. Kuzmich, K. Mølmer, and E. Polzik, Physical review letters **79**, 4782 (1997).
[28] T. Fernholz, H. Krauter, K. Jensen, J. F. Sherson, A. S. Sørensen, and E. S. Polzik, Physical review letters **101**, 073601 (2008).
[29] M. H. Schleier-Smith, I. D. Leroux, and V. Vuletić, Physical Review A **81**, 021804 (2010).
[30] E. G. Dalla Torre, J. Otterbach, E. Demler, V. Vuletic, and M. D. Lukin, Physical review letters **110**, 120402 (2013).
[31] A. Parkins, E. Solano, and J. Cirac, Physical Review Letters **96** (2006).
[32] J. Hald, J. Sørensen, C. Schori, and E. Polzik, Physical review letters **83**, 1319 (1999).
[33] C. Orzel, A. Tuchman, M. Fenselau, M. Yasuda, and M. Kasevich, Science **291**, 2386 (2001).
[34] V. Josse, A. Dantan, L. Vernac, A. Bramati, M. Pinard, and E. Giacobino, Physical review letters **91**, 103601 (2003).
[35] G.-B. Jo, Y. Shin, S. Will, T. Pasquini, M. Saba, W. Ketterle, D. E. Pritchard, M. Vengalattore, and M. Prentiss, Physical Review Letters **98**, 030407 (2007).
[36] J. Esteve, C. Gross, A. Weller, S. Giovanazzi, and M. K. Oberthaler, Nature **455**, 1216 (2008).
[37] P. Böhi, M. F. Riedel, J. Hoffrogge, J. Reichel, T. W. Hänsch, and P. Treutlein, Nature Physics **5**, 592 (2009).
[38] T. Takano, M. Fuyama, R. Namiki, and Y. Takahashi, Physical review letters **102**, 033601 (2009).
[39] I. D. Leroux, M. H. Schleier-Smith, and V. Vuletić, Physical Review Letters **104**, 073602 (2010).
[40] Z. Chen, J. G. Bohnet, S. R. Sankar, J. Dai, and J. K. Thompson, Physical review letters **106**, 133601 (2011).
[41] H. Krauter, C. A. Muschik, K. Jensen, W. Wasilewski, J. M. Petersen, J. I. Cirac, and E. S. Polzik, Physical review letters **107**, 80503 (2011).
[42] M. F. Riedel, P. Böhi, Y. Li, T. W. Hänsch, A. Sinatra, and P. Treutlein, Nature **464**, 1170 (2010), ISSN 0028-0836.
[43] W. Muessel, H. Strobel, D. Linnemann, D. Hume, and M. Oberthaler, Physical Review Letters **113**, 103004 (2014).
[44] L. Pezzè, A. Smerzi, M. K. Oberthaler, R. Schmied, and P. Treutlein, Reviews of Modern Physics **90**, 035005 (2018).
[45] W. Wasilewski, K. Jensen, H. Krauter, J. Renema, M. Balabas, and E. Polzik, Physical Review Letters **104** (2010).
[46] A. Louchet-Chauvet, J. Appel, J. J. Renema, D. Oblak, N. Kjaergaard, and E. S. Polzik, New Journal of Physics **12** (2010).
[47] G. Vasilakis, H. Shen, K. Jensen, M. Balabas, D. Salart, B. Chen, and E. Polzik, Nature Physics **11**, 389 (2015).
[48] J. Bohnet, K. Cox, M. Norcia, J. Weiner, Z. Chen, and J. Thompson, Nature Photonics **8**, 731 (2014).
[49] M. Ban, Journal of Optics B: Quantum and Semiclassical Optics **1**, L9 (1999).
[50] P. M. Anisimov, G. M. Raterman, A. Chiruvelli, W. N. Plick, S. D. Huver, H. Lee, and J. P. Dowling, Physical review letters **104**, 103602 (2010).
[51] S. L. Braunstein and P. Van Loock, Reviews of modern physics **77**, 513 (2005).
[52] B. Julsgaard, A. Kozhekin, and E. S. Polzik, Nature **413**, 400 (2001).
[53] K. Hammerer, A. S. Sørensen, and E. S. Polzik, Reviews of Modern Physics **82**, 1041 (2010), ISSN 0034-6861.

[54] M. Fadel, T. Zibold, B. Décamps, and P. Treutlein, Science **360**, 409 (2018), ISSN 0036-8075.
[55] P. Kunkel, M. Prüfer, H. Strobel, D. Linnemann, A. Frölian, T. Gasenzer, M. Gärttner, and M. K. Oberthaler, Science **416**, 413 (2018).
[56] K. Lange, J. Peise, B. Lücke, I. Kruse, G. Vitagliano, I. Apellaniz, M. Kleinmann, G. Tóth, and C. Klempt, Science **360**, 416 (2018).
[57] P. Treutlein, T. W. Hänsch, J. Reichel, A. Negretti, M. A. Cirone, and T. Calarco, Phys. Rev. A **74**, 022312 (2006).
[58] A. N. Pyrkov and T. Byrnes, New Journal of Physics **15**, 093019 (2013).
[59] D. Rosseau, Q. Ha, and T. Byrnes, Physical Review A **90**, 052315 (2014).
[60] M. I. Hussain, E. O. Ilo-Okeke, and T. Byrnes, Physical Review A **89**, 053607 (2014).
[61] Y. Jing, M. Fadel, V. Ivannikov, and T. Byrnes, New Journal of Physics **21**, 093038 (2019).
[62] O. Pettersson and T. Byrnes, Physical Review A **95**, 043817 (2017).
[63] S. Idlas, L. Domenzain, R. Spreeuw, and T. Byrnes, Physical Review A **93**, 022319 (2016).
[64] T. Byrnes, Physical Review A **88**, 023609 (2013), ISSN 1050-2947.
[65] H. Kurkjian, K. Pawłowski, A. Sinatra, and P. Treutlein, Physical Review A **88**, 043605 (2013).
[66] J. Kitzinger, M. Chaudhary, M. Kondappan, V. Ivannikov, and T. Byrnes, arXiv preprint arXiv:2006.03852 (2020).
[67] T. Byrnes, K. Wen, and Y. Yamamoto, Physical Review A **85**, 040306(R) (2012).
[68] T. Byrnes, D. Rosseau, M. Khosla, A. Pyrkov, A. Thomasen, T. Mukai, S. Koyama, A. Abdelrahman, and E. Ilo-Okeke, Optics Communications **337**, 102 (2015).
[69] A. Kuzmich and E. Polzik, Physical review letters **85**, 5639 (2000).
[70] J. Reichel and V. Vuletic, *Atom chips* (John Wiley & Sons, 2011).
[71] S. Whitlock, R. Gerritsma, T. Fernholz, and R. Spreeuw, New Journal of Physics **11**, 023021 (2009).
[72] A. Abdelrahman, T. Mukai, H. Hartmut, and T. Byrnes, Optics Express **22**, 195 (2014), ISSN 10944087.
[73] P. Bohi, M. F. Riedel, J. Hoffrogge, J. Reichel, T. W. Hansch, and P. Treutlein, Nat Phys **5**, 592 (2009), ISSN 1745-2473.
[74] J. M. Geremia, J. K. Stockton, and H. Mabuchi, Physical Review A **73**, 042112 (2006), ISSN 1050-2947.
[75] M. Kubasik, M. Koschorreck, M. Napolitano, S. R. de Echaniz, H. Crepaz, J. Eschner, E. S. Polzik, and M. W. Mitchell, Physical Review A **79**, 043815 (2009), ISSN 1050-2947.
[76] S. R. de Echaniz, M. W. Mitchell, M. Kubasik, M. Koschorreck, H. Crepaz, J. Eschner, and E. S. Polzik, Journal of Optics B: Quantum and Semiclassical Optics **7**, S548 (2005), ISSN 1464-4266.
[77] E. O. Ilo-Okeke and T. Byrnes, Physical review letters **112**, 233602 (2014).
[78] E. O. Ilo-Okeke and T. Byrnes, Physical Review A **94**, 013617 (2016), ISSN 2469-9926.
[79] H. F. Hofmann and S. Takeuchi, Phys. Rev. A **68**, 032103 (2003).
[80] M. D. Reid, P. D. Drummond, W. P. Bowen, E. G. Cavalcanti, P. K. Lam, H. A. Bachor, U. L. Andersen, and G. Leuchs, Reviews of Modern Physics **81**, 1727 (2009), ISSN 0034-6861.
[81] G. Adesso, T. R. Bromley, and M. Cianciaruso, Journal of Physics A: Mathematical and Theoretical **49**, 473001 (2016).
[82] Z.-H. Ma, J. Cui, Z. Cao, S.-M. Fei, V. Vedral, T. Byrnes, and C. Radhakrishnan, EPL (Europhysics Letters) **125**, 50005 (2019).
[83] J. F. Clauser, M. A. Horne, A. Shimony, and R. A. Holt, Phys. Rev. Lett. **23**, 880 (1969).
[84] E. Oudot, J.-D. Bancal, P. Sekatski, and N. Sangouard, New Journal of Physics **21**, 103043 (2019).
[85] O. Pettersson and T. Byrnes, Physical Review A **95**, 043817 (2017), ISSN 2469-9926.
[86] A. N. Pyrkov and T. Byrnes, New Journal of Physics **16**, 073038 (2014).
[87] A. N. Pyrkov and T. Byrnes, Physical Review A **90**, 062336 (2014).

Appendix A: Amplitude of a beam split coherent state

In this section we show that the coefficients $C_{n_c n_d}(\chi)$ given in (22) correspond to the Fock state amplitudes of a coherent state entering a beam splitter. Suppose a coherent state in mode a enters a beam splitter and exits into two modes according to the transformation

$$a = c\cos\chi + d\sin\chi. \tag{A1}$$

Then a coherent state of amplitude α transforms as

$$\begin{aligned}|\alpha\rangle_a &= e^{-|\alpha|^2/2} e^{\alpha\cos\chi c^\dagger + \alpha\sin\chi d^\dagger}|\text{vac}\rangle \\ &= |\alpha\cos\chi\rangle_c |\alpha\sin\chi\rangle_d \\ &= \sum_{n_c,n_d=0}^{\infty} C_{n_c n_d}(\chi)|n_c\rangle|n_d\rangle.\end{aligned} \tag{A2}$$

The last line shows the claimed relation.

Appendix B: Approximations involving the Jacobi theta function

Here we describe the approximations involved in obtaining the expression (33). The expression to be computed is

$$\mathcal{N} = \sum_{k_1,k_2=0}^{N} e^{-\frac{2}{N}\left[(k_1-\frac{N}{2})^2+(k_2-\frac{N}{2})^2\right]} e^{-n_c\tau^2(k_1-k_2)^2} \tag{B1}$$

For $N \gg 1$, we can safely extend the limits of the sums from $-\infty$ to ∞ as the first Gaussian factor strongly suppresses terms outside the region $0 \le k_1, k_2 \le N$. We first make a transformation of variables in terms of the relative and center of mass variables, defined as

$$\begin{aligned}k_r &= \frac{1}{2}(k_1 - k_2) \\ k_c &= \frac{1}{2}(k_1 + k_2 - N).\end{aligned} \tag{B2}$$

For integer k_r, k_c, this only covers half the points covered by k_1, k_2. Thus in order to cover all combinations of k_1, k_2, we must displace the k_1 variable by one unit. In these variables, the full set of points are then given according to

$$\mathcal{N} \approx \sum_{k_r,k_c=-\infty}^{\infty} \Big[e^{-\frac{4}{N}(k_r^2+k_c^2)-4n_c\tau^2 k_r^2} + e^{-\frac{2}{N}(2k_r^2+2k_c^2+2k_r+2k_c+1)-n_c\tau^2 k_r^2(4k_r^2+4k_r+1)} \Big] \tag{B3}$$

The sums over Gaussians function can be evaluated according to the expressions

$$\sum_{k=-\infty}^{\infty} e^{-xk^2} = \vartheta_3(0, e^{-x}) \tag{B4}$$

$$\sum_{k=-\infty}^{\infty} e^{-x(k^2+k)} = e^{x/4}\vartheta_2(0, e^{-x}), \tag{B5}$$

which gives (33).

We note that the Jacobi theta functions can be approximated to within 6 % accuracy using the expressions

$$\vartheta_3(0, e^{-x}) \approx \frac{1}{\sqrt{\tanh(x/\pi)}}$$
$$\vartheta_2(0, e^{-x}) \approx \frac{\operatorname{sech}(x/4)}{\sqrt{\tanh(x/\pi)}}. \tag{B6}$$

These functions interpolate between the behavior of the Jacobi theta functions for $x \ll 1$

$$\vartheta_3(0, e^{-x}) \approx \vartheta_2(0, e^{-x}) \approx \sqrt{\frac{\pi}{x}} \tag{B7}$$

and $x \gg 1$

$$\vartheta_3(0, e^{-x}) \approx 1$$
$$\vartheta_2(0, e^{-x}) \approx 2e^{-x/4}. \tag{B8}$$

Appendix C: Transformation between Fock states in different bases

The Fock eigenstates of the spin operators corresponding to S^x and S^y are given by

$$|k\rangle^{(x)} = e^{-iS^y\pi/4}|k\rangle$$
$$|k\rangle^{(y)} = e^{-iS^z\pi/4}e^{-iS^y\pi/4}|k\rangle. \tag{C1}$$

Here the matrix elements of the S^y rotation are given by

$$\langle k|e^{-iS^y\theta/2}|k'\rangle = \sqrt{k'!(N-k')!k!(N-k)!}$$
$$\times \sum_n \frac{(-1)^n \cos^{k-k'+N-2n}(\theta/2)\sin^{2n+k'-k}(\theta/2)}{(k-n)!(N-k'-n)!n!(k'-k+n)!}, \tag{C2}$$

where $|k\rangle$ and the eigenstates of S^z. The matrix elements of S^x are accordingly given by

$$\langle k|e^{-iS^x\theta/2}|k'\rangle = i^{k'-k}\langle k|e^{-iS^y\theta/2}|k'\rangle \tag{C3}$$

where we used the fact that $S^x = e^{-iS^z\pi/4}S^y e^{iS^z\pi/4}$.